Mid-infrared supercontinuum generation from 2 to 14 μm in arsenic-and antimony-free chalcogenide glass fibers

Arnaud Lemiere, Frédéric Désévédavy, Pierre Mathey, Paul Froidevaux, Grégory Gadret, Jean-Charles Jules, Christophe Aquilina, Bertrand Kibler, Pierre Béjot, Franck Billard, et al.

Mid-infrared supercontinuum generation from 2 to 14 µm in various arsenic- and antimony-free chalcogenide glass fibers

ARNAUD LEMIERE, FREDERIC DESEVEDAVY, PIERRE MATHEY, PAUL FROIDEVAUX, GREGORY GADRET, JEAN-CHARLES JULES, CHRISTOPHE AQUILINA, BERTRAND KIBLER, PIERRE BEJOT, OLIVIER FAUCHER AND FREDERIC SMEKTALA*

Laboratoire Interdisciplinaire Carnot de Bourgogne (ICB), UMR6303 CNRS – Université Bourgogne Franche-Comté, Avenue Alain Savary, 21000 Dijon (France).
**frederic.smektala@u-bourgogne.fr*

Abstract: We demonstrate the fabrication of arsenic- and antimony-free chalcogenide glasses compatible with glass fiber processing. Optical fibers with distinct index profiles are presented and characterized, namely single material fibers with or without a suspended core and standard step-index fibers with varying core diameter. In addition, we evidence their potential for nonlinear photonic devices in the mid-infrared spectral region by means of supercontinuum generation experiments in the femtosecond regime. Spectral broadenings are obtained, extending on several octaves in the mid IR from 2 to 14 µm.

OCIS codes: (000.0000) General; (000.2700) General science.

1. Introduction

Mid-infrared (mid-IR) supercontinuum (SC) sources covering ~2–16 µm are of great interest for many applications in defense, medical [1] and particularly for sensing. In this spectral region, organic compounds such as biomolecules present fundamental vibrational resonances and an absorption pattern corresponding to their spectroscopic fingerprints [2, 3]. Furthermore, this spectral range covers the strategic atmospheric windows 3-5 µm and 8-12µm. This is particularly interesting for practical applications such as greenhouse gases sensing [4], chemical sensing, medical therapeutics and food safety monitoring [3]. Besides, it is worth mentioning that many applications of optical technologies related to healthcare, pharmaceuticals, and environmental monitoring are calling for biocompatible materials excluding compounds containing arsenic as well as antimony. Arsenic and its compounds are known to be highly toxic substances. Antimony has a similar chemical behavior in particular from the biological point of view [5]. According to toxicological data, carcinogen effects are attributed to antimony oxide. In addition As, Sb and their compounds are known to be major pollutants for outer environment especially when these substances pollute drinkable water [5, 6]. The European REACH [7] (Registration, Evaluation, Authorization and Restriction of Chemicals) regulation aims to limit or suppress as far as possible the usage of highly toxic substances. Presently arsenic is already classified as acutely toxic in REACH database. It is also considered as one of the tenth substances of major concerns for human health by the World Health Organization. Because of toxicological data that are judged incomplete or too old, antimony is currently not classified. However, based on experimental data on representative samples and on the comparison with the di-antimony trioxide known as carcinogen, an alternative proposal for the classification and labeling of antimony is provided by REACH [7]. Moreover, arsenic and antimony surfaces exposed to room atmosphere lead to formation of the corresponding carcinogen oxides. Thus, security issues may occur during glass preparation, fiber drawing, and performance testing [8, 9, 10].

Arsenic and antimony are known to increase glass formation region [11] as well as refractive and nonlinear indices [12, 13]. Indeed, most of SC spectra reported in chalcogenide glass (ChG) fibers are obtained with sulfide, selenide or telluride based compositions containing arsenic and/or antimony such as As_2S_3 [14], As_2Se_3 [15, 16], GeAsS,GeAsSe [17, 18], GeAsSeTe [19, 20], GeSbS(Ga), GeSbSe [17]. To the best of our knowledge, only one study reports SC obtained with a ChG fiber free of arsenic and antimony [2]. Such ChG glasses (ChGs) compatible with fiber drawing operations and allowing for SC generation are even less common. We can cite the work of [2] based on an As and Sb-free core glass containing iodine (but with a Sb-containing clad glass) difficult to process in particular during the drawing because of iodine degassing and phase separation issues [21].

In the present work, we demonstrate the fabrication of single material optical fibers as well as step-index ones based on ChGs free of highly toxic elements such as arsenic and antimony. The studied compositions belong to the Ge-Se-Te ternary system for both core and cladding glasses. This system has already been studied for optical fibers preparation [22, 23, 24, 25] and thin films [26]. Despite the fact that previous works explored the full ternary diagram especially for thin films, to the best of our knowledge, no result about low-losses (<5dB/m) step-index fibers has been yet reported. Until now, step-index fibers losses exceed 10dB/m [27, 24]. Indeed, compared with S- or Se-based glasses, Te-based ChGs are of interest for mid-IR SC generation since they present higher optical nonlinearities and broadest transmission windows due to the higher atomic weight of Te [12, 28]. Nevertheless, the metallic character of Te leads to a greater tendency for crystallization, which prevents the production of low-losses optical fibers because of high scattering [29]. The substitution of a small amount of Te by Se increases the resistance to crystallization while retaining a wide optical transmission window. But to date the attenuation of such fibers is still high (>10 dB/m) and the drawing is difficult to control [23, 24].

From this state of the art, we study in this work two compositions belonging to the pseudo binary $GeSe_4$ – $GeTe_4$, on the Se rich side. The thermal and optical properties of bulks and fibers have been investigated as well as the purification process, in order to obtain low-losses optical fibers. The present work also evidences dispersion engineering in step-index and suspended-core fibers drawn from these glasses, according to their opto-geometric characteristics, in particular for optimizing SC generation. As a result, we are able to present here the first results of SC generation with such fibers. In particular, a very large SC spectrum, spanning from 2 to 14 µm, is obtained with a 10-µm core diameter step-index fiber.

2. Glasses and fibers processing

2.1 Glass composition

$GeSe_4$ glass is known to be compatible with fiber technology, from glass purification through distillation procedures to drawing operations [30]. Addition of $GeTe_4$ increases several important parameters, namely the glass transition temperature, the refractive index and the Kerr coefficient [26]. Some of the main thermal and optical properties of $GeSe_4$ and $GeTe_4$ glasses are gathered in Table 1. However, glass compositions from the Te-rich side of the pseudo binary $GeSe_4$ - $GeTe_4$ being difficult to process, single material fibers are hardly obtained and exhibit high losses (>10 dB/m), far from requirements for SC generation and other applications [23, 22, 24]. Consequently, we focused our work on the Se-rich part of the pseudo-binary (Fig.1). The cladding and core compositions are $Ge_{20}Se_{70}Te_{10}$ (87,5% $GeSe_4$ – 12,5% $GeTe_4$) and $Ge_{20}Se_{60}Te_{20}$ (75% $GeSe_4$ – 25%$GeTe_4$) respectively. In the following, these two compositions are indifferently called GST glasses.

Table 1. Thermal and optical properties of $GeSe_4$ and $GeTe_4$ glasses

Glass	T_g(°C)	T_x(°C)	n @ 3 µm	Band gap (µm)	n_2 (10^{-18} $m^2.W^{-1}$)
$GeSe_4$	160 [30]	-	2.419 [31]	0.730[a] [32] 0.650[b] [26]	3.2 @ 1.55 µm [32]
$GeTe_4$	140 [33]	217 [33]	3.353 [34]	1.5[b] [26]	No data

[a]: bulk, [b]: thin film

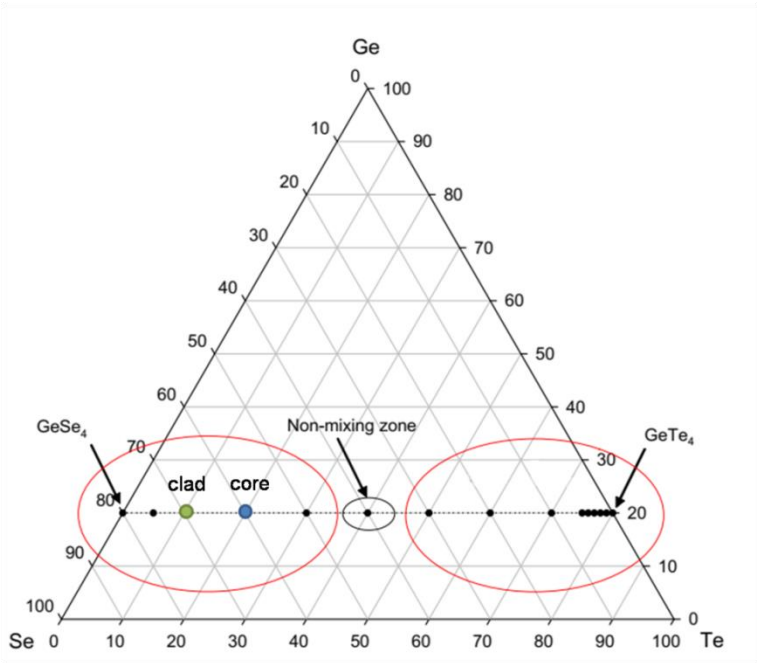

Fig.1. Ternary Ge-Se-Te diagram reproduced from [23]. Red circles stand for glass forming regions. Core and cladding compositions are indicated.

2.2 Glass synthesis and purification

The starting elements are 5N bulky Ge and Te from Umicore. Se is 5N pellets from Alfa Aesar. After weighing of stoichiometric quantities, all three elements were inserted into silica ampoules which were evacuated to 1 x 10^{-5} mbar for several hours. Under such a secondary vacuum, Te and Se containing ampoules were heated up to 430°C and 230°C, respectively, in order to remove TeO_2 and SeO_2 superficial oxides. Germanium was heated up to 600°C to remove free water adsorbed on the raw material surface. Then, the precursors are gathered in the same ampoule in which 50 ppm (wt) of Al and 1000 ppm (wt) of $TeCl_4$ are added for further purification. Al is used as an oxygen getter; during synthesis, it reduces remaining oxides in the batch, to form alumina (Al_2O_3). $TeCl_4$ is used as a hydrogen getter; it reacts with remaining hydrogenated entities to form HCl. Because reaction with $TeCl_4$ can be reversible, the glass is quenched from a sufficiently high temperature to preserve the purification stage [35]. In the next step, the glass is annealed and then distilled under dynamic vacuum by means of two furnaces, a turbo molecular vacuum pump, and a cooled trap, see Fig. 2a. As a refractory, alumina is not distillated and stays in the starting ampoule, in furnace 1. As a gas, HCl is evacuated and trapped in the liquid nitrogen cooled trap. At the end of the distillation

stage, the GST glass has moved in the second ampoule, in furnace 2. Then, this ampoule is sealed and placed in a two-zone furnace, furnace 3 (Fig. 2b), for a static distillation of the GST glass which leaves the traces of refractory particles (C, Al_2O_3 or SiO_2) responsible for optical scattering [36, 37] in the left side of the ampoule, when the glass moves to the right side of the ampoule (Fig. 2b). Finally, after sealing the right side ampoule, the glass batch is inserted into a rocking furnace for the refining process at 850°C for 10 hours (Fig. 2c), and then quenched and annealed at T_g – 5°C for 12h.

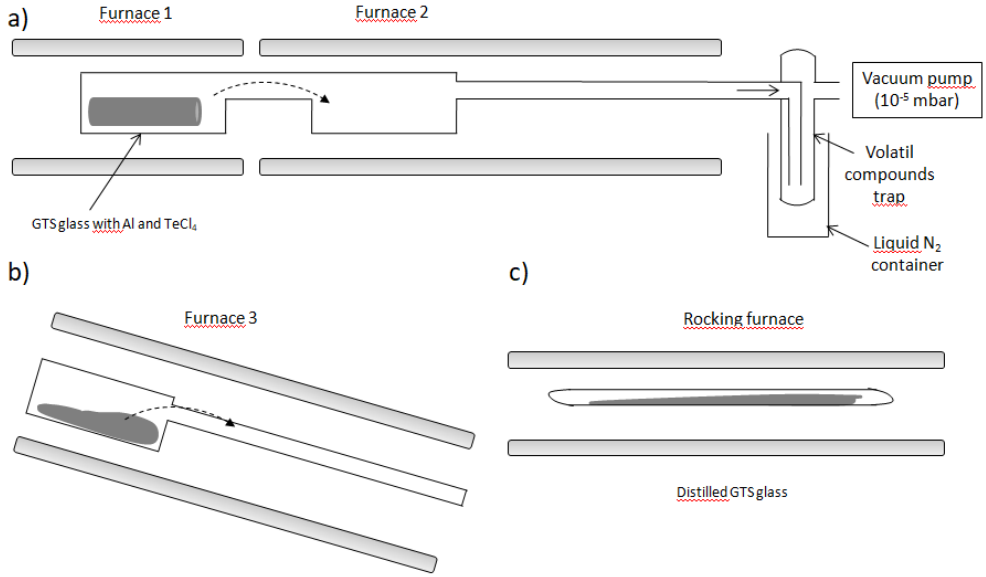

Fig. 2. Scheme of glass purification steps, a) distillation, under dynamic secondary vacuum, of the glass containing oxides and hydrogen getters (Al and $TeCl_4$), b) distillation under static vacuum of the previous distillate, c) refining step in order to obtain the final glass.

2.3 Glass optical fibers fabrication

We have already described the drawing steps in previous papers. Step-index fibers were fabricated by means of the rod-in-tube method [38, 39]. First, a 8-cm-long rod with16 mm outer diameter is stretched down to 900 µm glass cane which is then inserted in a drilled clad perform, thus providing the suitable preform to draw step-index fiber with 100-350 µm outer diameter (i.e., corresponding to a core diameter varying from 6 to 20 µm). During these two operations, single material fibers made from both the core and cladding glasses are also drawn in order to measure the material losses by the cut-back technique (see section 3.2.1). We also fabricated suspended core fibers by means of the mechanical drilling method on initial rods from core glass, with a 16 mm outer diameter [14]: after annealing, a glass rod was drilled to obtain three holes of typically 1 mm diameter and 30 mm length, thus leading to the air-suspended structure with three fine struts supporting the suspended core (see further Fig. 7a). The resulting perform is then drawn into fiber under a nitrogen gas pressure to control the hole size.

3. Characterization

3.1 Thermal properties

Differential scanning calorimetry measurements (DSC 2920 TA Instrument) were performed on core and cladding glasses in order to determine the glass transition temperature T_g. DSC curves were registered in the 20°C–400°Crange using typical 10–20 mg bulk glass samples heated at a rate of 10°C/min under N_2 gas flow (50 mL/min). Glass transition temperature and

drawing temperature of these two glasses are given in Table 2. No sign of crystallization was observed on both compositions.

Table 2. Thermal properties of GST core and clad glasses

Composition	T_g (°C)	Drawing temperature (°C)[a]
$Ge_{20}Se_{60}Te_{20}$ (core)	162	430
$Ge_{20}Se_{70}Te_{10}$ (clad)	159	430

[a]: *temperature given by the thermocouple placed in the vicinity of the glass during drawing.*

3.2 Linear optical characterization

3.2.1 Transmission and attenuation

After polishing 5-mm-thick glass samples using SiC papers and diamond suspension, mid-IR bulk transmissions were measured with a FTIR Perkin Elmer spectrometer (Spectrum One), while the near-infrared transmission was measured with a Perkin Elmer Lambda 900 spectrometer. Transmission spectra of purified core and cladding compositions are shown in Fig. 3. The bandgap wavelength is determined for an absorption of 10 cm^{-1} and is equal to 1.02 and 0.89 µm for core and cladding glass respectively. In both cases, multiphonon absorption stops the transmission around 17 µm and one can notice that resonances are observed at 11 µm and above.

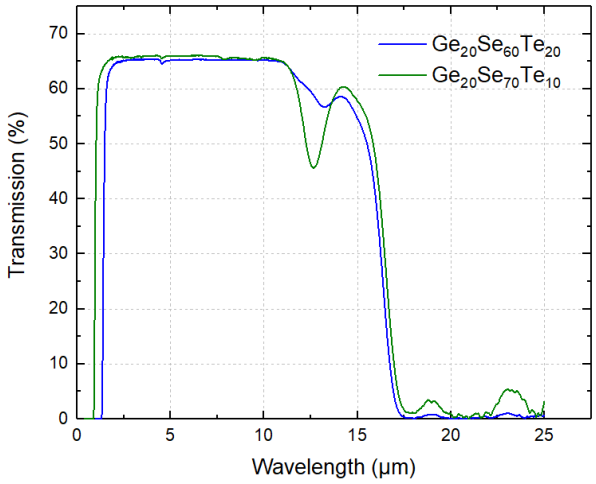

Fig. 3. Transmission of core and cladding glasses obtained from 5-mm-thick bulk samples

The infrared attenuation spectra of the single material fibers were determined by using the cutback method on several meters-long fiber samples with a Fourier Transform Infrared (FTIR) spectrometer (NICOLET 6700) working in the 1–4.5 µm range. For technical purposes, an external halogen lamp emitting from 0.4 to 4.5 µm was used as the light source. For longer wavelength we used a Perkin Elmer (Spectrum One) spectrometer allowing a measurement between 1.3 and 25 µm. Because of the light source low power of the latter spectrometer (black body Globar) only attenuation of the purified glass fibers can be measured with this spectrometer. Figure 4 compares measured losses for single material

fibers made from the purified core and clad glasses. Thanks to distillations procedures the losses are strongly decreased, even below 2 dB/m over a very large spectral range, when oxides and hydrogenated entities are removed or at least deeply reduced. The remaining Se-H groups are responsible for the absorption band centered at 4.5 µm. According to Se-H attenuation coefficient, $\varepsilon_{Se\text{-}H}$ = 1 dB/m/ppm(at) [43, 36], we estimated the residual quantity of Se-H groups to 8 ppm(at) corresponding to the same order of magnitude than previously reported results [36, 37, 30].

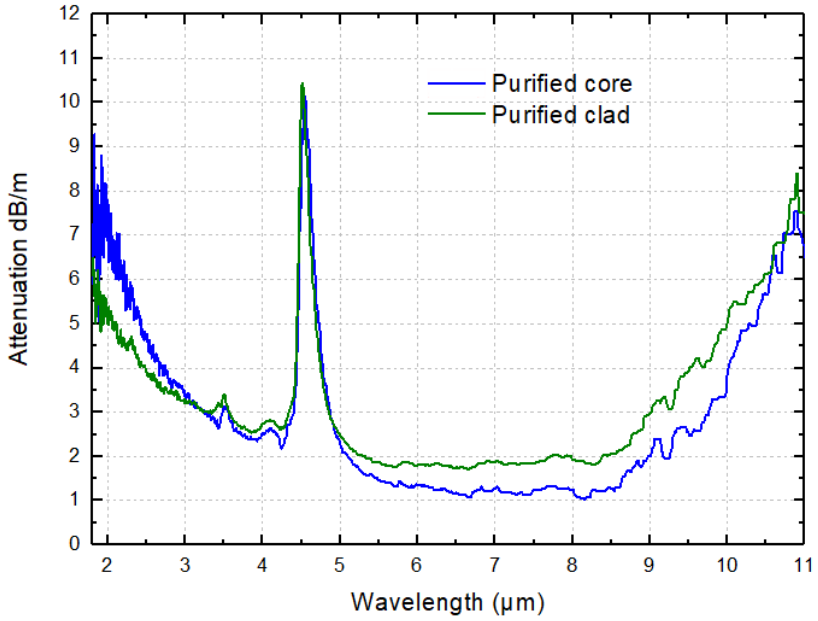

Fig. 4. Infrared attenuation spectra of single material fibers made of purified core and cladding glasses.

3.2.2 Refractive indices

Refractive index values of both glass compositions (ternary systems) were calculated based on the Clausius Mossoti relation [40] and the use of refractive index measurements reported in literature on binary systems, namely $GeSe_4$ [31] and $GeTe_4$ [34] glasses. Indeed, the core and cladding glasses are expressed as stoichiometric mixtures of $GeSe_4$ and $GeTe_4$. Core glass $Ge_{20}Se_{60}Te_{20}$ corresponds to $0.75GeSe_4 - 0.25GeTe_4$ and cladding glass $Ge_{20}Se_{70}Te_{10}$ corresponds to $0.875GeSe_4 - 0.175GeTe_4$ (mol). The resulting wavelength dependences of core and cladding refractive indices are plotted in Fig. 5. These curves can be well fitted by two-pole Sellmeier equations (see Eq.(1)), and the corresponding Sellmeier coefficients are listed in Table 3. The refractive index difference is found to be $\Delta n = 8.9 \times 10^{-2}$ at 5 µm. Based on this simple step-index profile, our fibers do not exhibit a strictly single-mode behavior in the mid-IR spectral range, but high numerical apertures and a rather strong confinement of the fundamental guided mode.

$$n^2 = 1 + \sum_{i=1}^{i=2} \frac{A_i \lambda^2}{\lambda^2 - A_i} \qquad (1)$$

Table 3. Sellmeier coefficients for $GeSe_4$, $GeTe_4$ and GST glasses

Glass composition	A_1	A_2	λ_1 (µm)	λ_2 (µm)
$GeSe_4$ [31]	4.813	0.126	0.278	19.738
$GeTe_4$ [34]	9.943	0.318	0.522	18.298
$Ge_{20}Se_{60}Te_{20}$	5.677	0.215	0.331	21.322
$Ge_{20}Se_{70}Te_{10}$	5.225	0.202	0.298	21.606

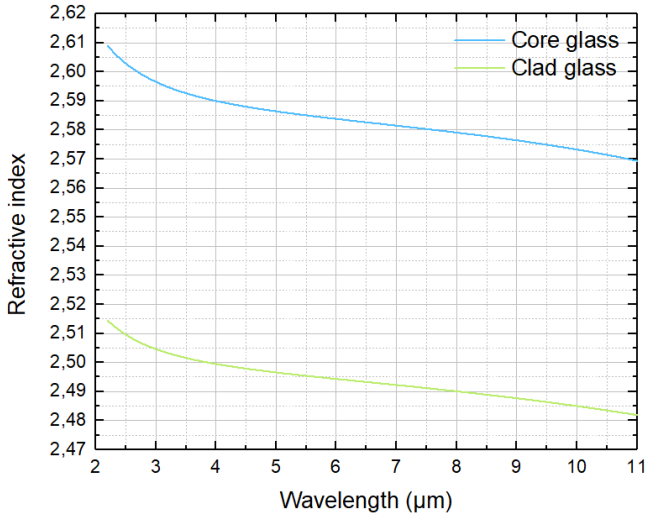

Fig. 5. Calculated refractive index as a function of wavelength for both core and cladding glasses.

3.2.3 Simple dispersion management of step-index fibers

Based on a simple step-index profile, we studied the corresponding dispersive properties of the fundamental mode propagating in our chalcogenide fibers with different core diameters. Dispersion curves, shown in Fig. 6, were obtained by solving the dispersion equation (also called the eigenvalue equation) for cylindrical step-index waveguides. An uncertainty of $\pm 10^{-2}$ on the refractive index difference (Δn) between core and cladding is taken into account to roughly estimate the impact of potential discrepancies between our numerical predictions and the genuine refractive indices of the fabricated glasses, hence we plot three dispersion curves for each core diameter. For a core diameter ranging from 6 to 14 µm, we observe that our fiber can exhibit distinct dispersive properties such as an all-normal dispersion (ANDi) profile or even a two-zero dispersion wavelength (ZDW) dispersion profile. By simply tuning the core diameter during fiber drawing, we are able to manage the group-velocity dispersion (GVD) of the fundamental guided mode ranging from all-normal dispersion (e.g., Φ_{core} = 6 µm) to multi-ZDW GVD profile (e.g., Φ_{core} = 10 µm). A standard single-ZDW dispersion profile is then found for larger core diameters (e.g., Φ_{core} = 14 µm). Consequently, various nonlinear propagation regimes can be explored to optimize SC generation [47]. It is worth noting that for a 10-µm core diameter, depending of Δn value the multi-ZDW profile is somehow uncertain but nearly flat and low anomalous dispersion is confirmed over a wide spectral range. For wavelengths below 4 µm, whatever the core diameter, the large normal dispersion is fixed to the bulk dispersion (core glass). Note that simple single-material fiber with large diameter exhibits the same dispersion properties than the bulk.

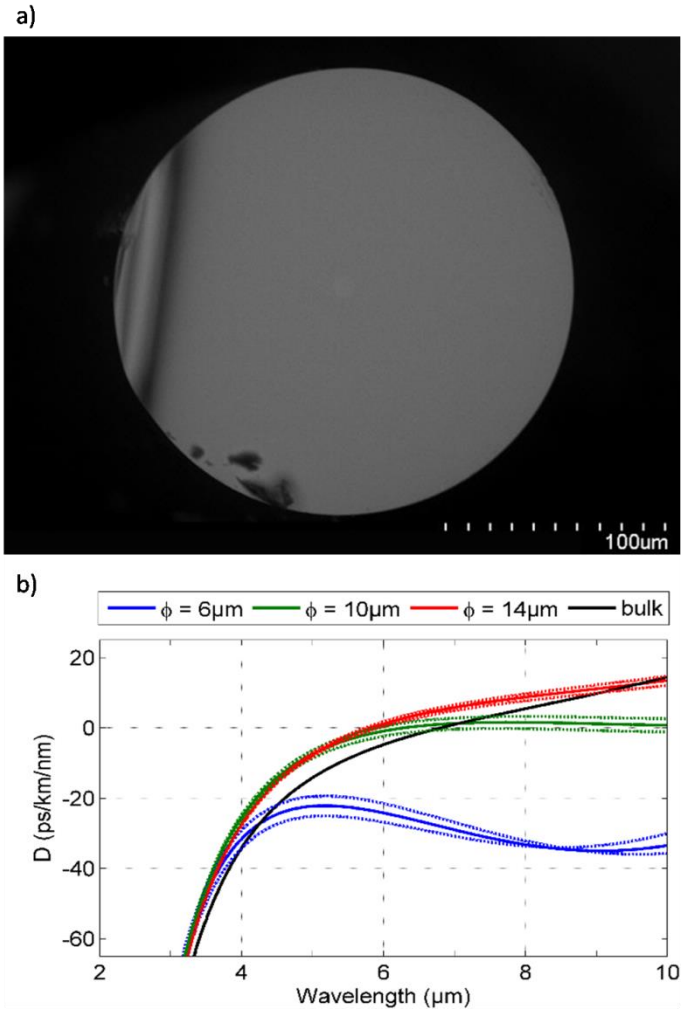

Fig. 6. (a) Profile of the chalcogenide step-index fiber with 10-µm core diameter and captured by means of a scanning electron microscope (SEM). (b) Calculated wavelength-dependent dispersion D of the fundamental guided mode in our step-index fibers with varying core diameter ϕ =6, 10, and 14µm. The solid black line indicates the chromatic dispersion from the core glass ($Ge_{20}Se_{60}Te_{20}$). Additional dashed curves give an estimate of possible dispersion variations induced by the uncertainty on refractive index difference for our glass pair.

3.2.4 Dispersion of suspended core fibers

Regarding the linear characteristics of suspended core fibers, we performed numerical simulations of modal properties based on the fiber geometry derived from the SEM analysis and by means of commercial software using a fully vectorial finite-element model. Fig. 7 shows the wavelength-dependence of dispersion parameter D for the fundamental guided mode for distinct values of the core diameter. We clearly observe the benefit of the strong light confinement offered by the suspended-core geometry, namely the easy blue-shift of the zero-dispersion wavelength when compared to step-index configuration. However, the strong decrease of the core size required to shift the ZDW below 3 µm would lead to significant coupling issues. But, with a 6-µm core diameter, there is a possibility to pump in the

anomalous dispersion regime at wavelengths about 3.7 µm contrary to the step-index fiber geometry (see Fig. 6). Such small-core fibers could be suitable for the development of compact SC sources when considering recent sub-200 fs laser sources operating between 2.8 and 3.6 µm based on fluoride fiber with high peak powers [45, 46]. In the following experiments, we make use of a suspended core fiber with 12.7 µm core diameter. In that case, the ZDW was already shifted in a significant manner, at wavelengths around 5 µm. Note that the blue-shift of ZDW is 1 µm further than for small-core step-index fibers studied in Fig. 6.

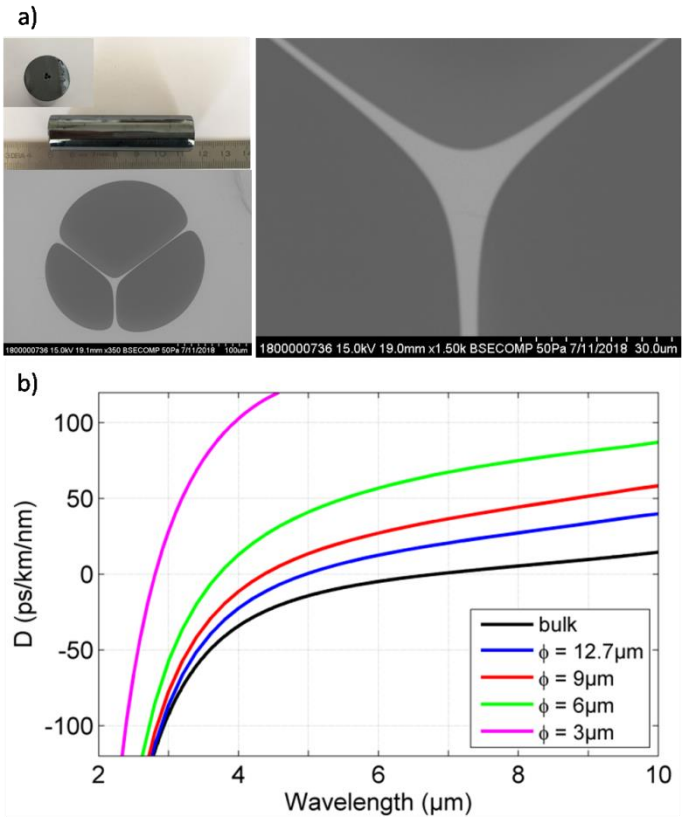

Fig. 7. (a) Picture of the three holes drilled preform and profile of the 12.7-µm suspended-core chalcogenide fiber captured by means of a scanning electron microscope (SEM).(b) Calculated wavelength-dependent dispersion D of the fundamental guided mode in our suspended core fibers with varying core diameter ϕ =3, 6, 9, and 12.7µm. The solid black line indicates the chromatic dispersion from the core glass ($Ge_{20}Se_{60}Te_{20}$).

4. Supercontinuum generation

4.1. Experimental set up

Fig.8 shows the experimental setup implemented for supercontinuum generation in our chalcogenide fibers. The high-power femtosecond pulses, with tunable central wavelength from 3.5 to 11µm, are delivered by a non-collinear optical parametric amplifier (NOPA) followed by a difference frequency generation (DFG) module. The NOPA is pumped by a chirped pulse amplified (CPA) Ti:sapphire system which delivers pulses centered at 790 nm with 3.2 mJ energy (100 fs pulse duration) at 1 kHz repetition rate. The maximum energy of the short-wave infrared pulse delivered by the DFG module is about 15 µJ, and the pulse duration is estimated to be 65 fs. Pump spectra for several wavelengths are shown in Fig. 9. The infrared beam is focused with a 6 mm focal length ZnSe objective into 40-mm-long segments of ChG fibers. The fiber mounted on a translation stage is placed in the position

maximizing the spectral bandwidth of SC generation. At this stage, the output SC is collimated with a ZnSe objective (f = 12 mm) and then focused with a gold coated parabolic mirror (f = 88.9 mm) on the input slit of the monochromator. Our Newport Cornerstone™ 130 1/8 m motorized monochromator is equipped with two diffraction gratings adapted for the wavelength range of interest. The first one (300 l/mm) is used in the 1.1–2.5 µm range with a peak efficiency of 90 % at the 1700 nm blaze wavelength, thus providing a spectral resolution of almost **5 nm.** The second one (150 l/mm) is used in the 2.5–12µm range with a peak efficiency of 75 % at the 5000 nm blaze wavelength**,** allowing a spectral resolution twice lower than the first one. SC light at the output slit is imaged by means of a gold coated parabolic mirror (f = 50.8 mm) on the liquid nitrogen-cooled HgCdTe detector. The detector signal is then extracted by means of a box car operating at the laser repetition rate. Higher diffraction orders were filtered out using various germanium-based long-pass filters. Accordingly, the spectrum is sequentially recorded with Ge-based long-pass filters placed before the detector and transmitting above 1.5, 2, 3, 5,7 and 9 µm, respectively. The full SC spectrum is then reconstructed by gathering the filtered spectra.

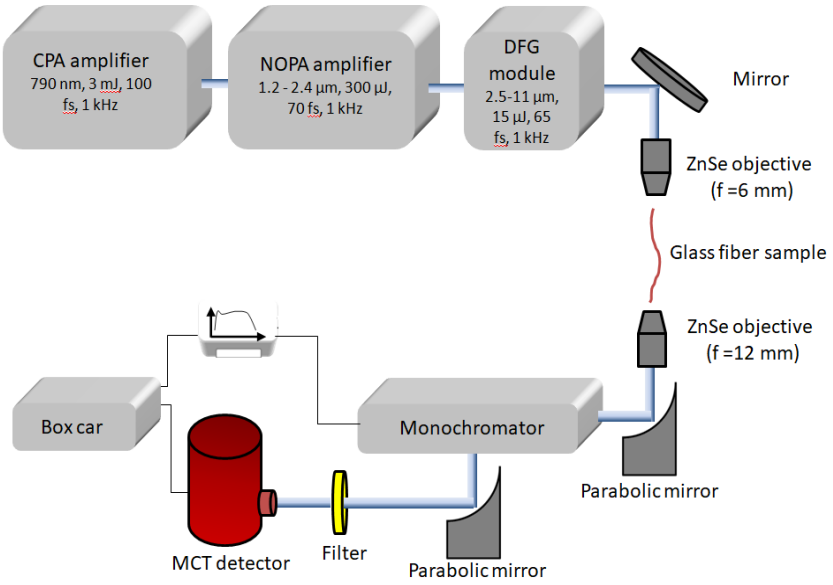

Fig.8. Experimental setup used for supercontinuum generation in our chalcogenide fibers free of arsenic and antimony.

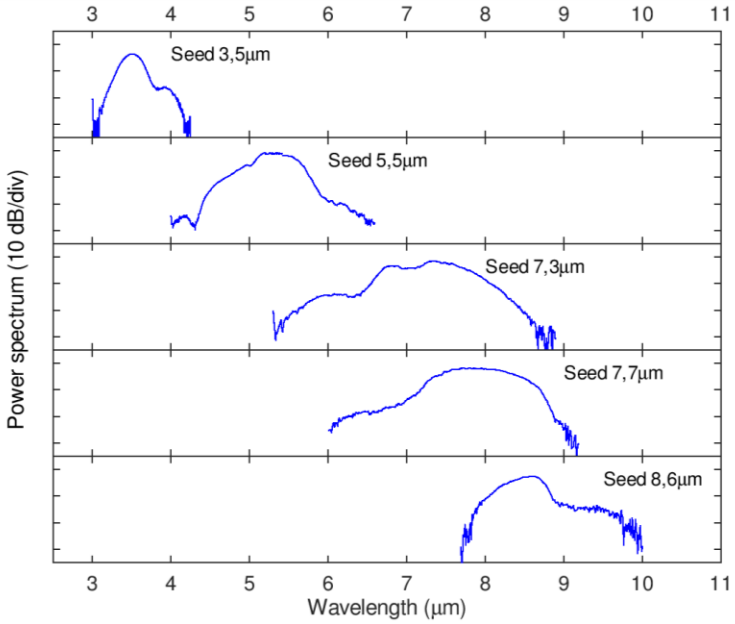

Fig. 9. Pump spectra for different wavelengths delivered by the fs source.

4.2 Single-material fibers

SC generation was first investigated in our single-material fiber (outer diameter equal to 210 µm) made of the core glass $Ge_{20}Se_{60}Te_{20}$ (see Fig. 10). Experimental SC spectra were obtained for the maximum average power available at distinct pumping wavelength. As the power decreases for increasing pump wavelength, one can notice the strong impact of the power on the resulting SC bandwidth [2]. However, we reveal that, even pumping in the large normal dispersion regime (far from the ZDW around 7 µm), SC generation (more particularly self-phase modulation) is efficient enough to cross the ZDW and to cover the spectral region between 2 and 10 µm approximately (see pumping wavelengths fixed at 3.5 and 5.5 µm). The spectral broadening becomes asymmetric relative to the initial pump wavelength, significant broadening is then observed in the anomalous dispersion regime where solitons can be formed and undergo Raman self-frequency shift [47]. On the contrary when the power decreases, whatever the wavelength the spectrum does not change significantly.

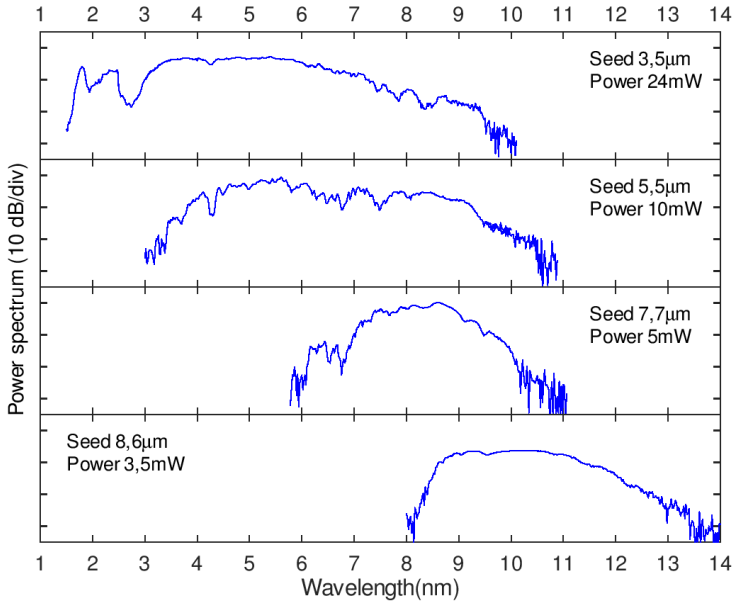

Fig. 10. Experimental SC obtained for different pumping wavelength (3.5, 5.5, 7.7 and 8.6 µm) in a single index fibers.

4.3 Step-index fibers

The present flexibility in the design of GVD properties for step-index fibers combined with strong optical confinement and our tunable fs pumping allows us to investigate an overview of relevant configuration of SC generation. First, we investigated SC generation in the two-ZDW fiber (i.e., 10 µm core diameter) for distinct pumping wavelengths with the same input power. The average pump power was measured just before the ZnSe coupling objective about 3.5 mW for pumping at 3.5 µm and 8.6 µm. For technical reason, we were not able to decrease the input power below 5 mW when pumping at 7.7 µm. Note also that for 8.6 µm pumping we cannot increase the power above 3.5 mW. For sake of clarity we present SC results for only 3 different pump wavelength in Fig. 11. Even with average power higher than 5 mW, the SC spectrum pumped at 5.5 µm (not shown here) is not as broad as the one pumped at 7.7 µm. All this is corroborated by numerical predictions of the fiber dispersion curve shown in Fig. 6b. Indeed the pumping at 7.7 µm in the low anomalous dispersion regime surrounded by two ZDWs provides optimized dispersion features for SC development. The spectral broadening reaches the maximum bandwidth mainly driven by soliton dynamics and the formation of dispersive waves (DWs) in both regions of normal dispersion far from the pump (induced by the presence of the two ZDWs) [47], namely below 6 µm and beyond 10-11 µm. When pumping at 3.5 µm in the normal dispersion regime, SC generation is mainly driven by self-phase modulation (SPM), and the spectrum remains nearly narrow and symmetric until crossing the ZDW and entering in the anomalous regime where solitons are formed and red shifted. Now when pumping at 8.6 µm still in the anomalous dispersion regime but close to the second ZDW, we observe that spectral broadening remains limited and even less efficient than 3.5-µm pumping with same incoming power. As the core diameter is 10 µm, we suppose that the coupling is less efficient at a wavelength of 8.6 µm.

Similar pumping configuration in between the ZDWs was also found to optimize SC generation in step-index tellurite fibers [48]. The largest SC spectrum here spans from 2 up to nearly 14 µm (-30 dB bandwidth). It is worth mentioning that our detection setup is not fully optimized for wavelengths above 12 µm so that SC may easily extend up to 14 µm and beyond. More precisely, the second grating has a degraded efficiency above 12 µm and the

sensitivity of the MCT detector drops after 12 µm. For future works beyond these proof-of-principle experiments, a third grating is then necessary as well as a MCT with a larger wavelength range towards the mid-IR.

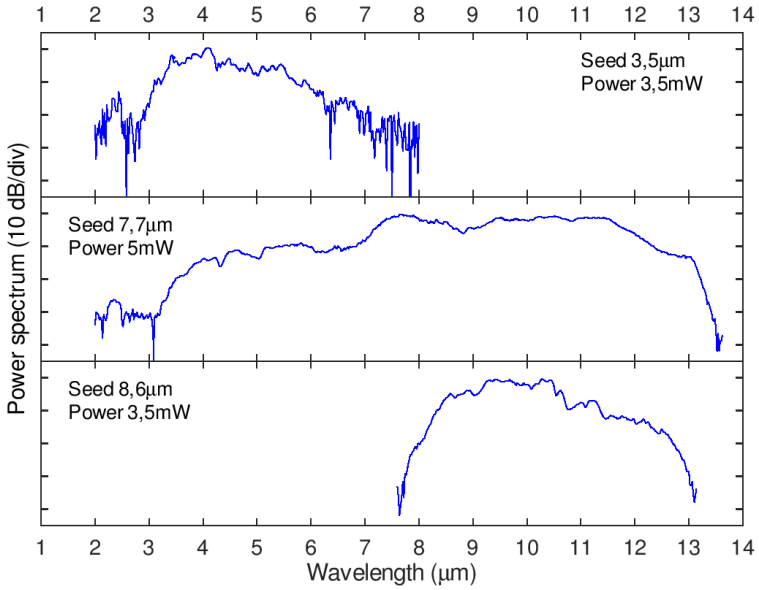

Fig. 11. Experimental SC spectra obtained with 10-µm-core chalcogenide step-index fiber and different pumping wavelength (3.5, 7.7 and 8.6 µm).

Next, we studied different step-index fibers with varying core diameters, namely 6, 10, and 14 µm. As shown by Fig. 12, we achieved the broadest SC spectrum by using the 10-µm core fiber. This confirms again the strong impact of dispersion profiles, which drives the nonlinear pulse propagation regime and the subsequent SC bandwidth. Indeed, a 10-µm core diameter corresponds to a rather flat dispersion curve associated to multi-ZDW features contrary to the 6-µm core fiber that exhibits a typical ANDi profile. For the latter, whatever the pumping wavelength, narrow spectral broadenings are expected (i.e., SPM only occurs in the normal dispersion). By using a 14-µm core fiber, we almost recover a very large SC spectrum spanning from 3 to 13 µm. In that case, the single ZDW dispersion profile and the pumping into the anomalous dispersion lead to soliton-driven SC generation associated with DWs (only on the short wavelength edge). No dispersive wave is generated on the long wavelength edge since the second ZDW is further shifted in the mid-IR and even does not exist. Consequently, the SC bandwidth is reduced when increasing the fiber core diameter, in particular due to the larger anomalous dispersion that restrains soliton dynamics.

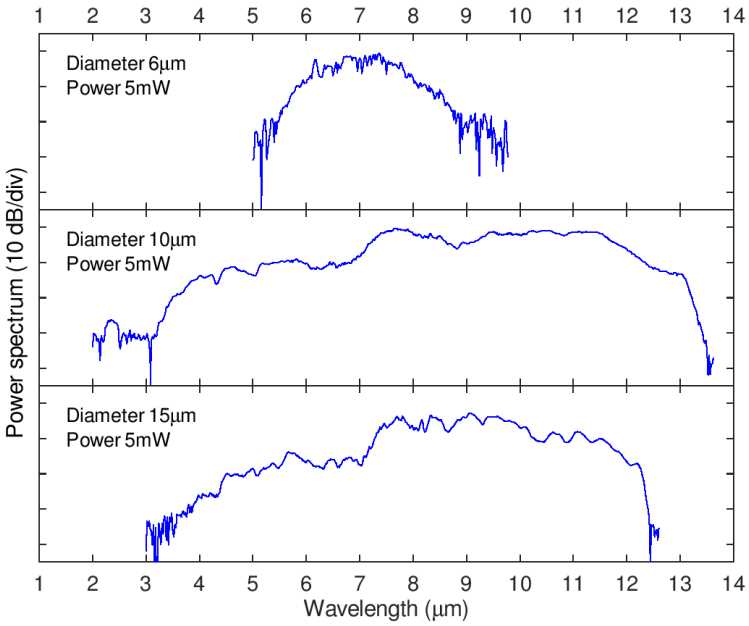

Fig. 12. Experimental SC spectra obtained in chalcogenide step-index fibers with different core diameter (6, 10 and 14 µm) by means of pumping at 7.7 µm.

4.4 Suspended core fibers

Finally, we report SC spectra obtained at the output of our chalcogenide suspended core fiber (12.7-µm core diameter) in Fig.13, in particular for two pump wavelengths 3.5 and 5.5 µm. The average pump power, measured just before the coupling objective, is respectively 5 and 10 mW. Our results are supported by the predicted dispersion curves shown in Fig. 7 indicating that the ZDW is located at 5 µm for this core diameter. The largest SC spectrum roughly spans from 3 to 12 µm, and it is obtained for the pump fixed at 5.5 µm corresponding to the anomalous dispersion of the fiber and close to its ZDW. When pumping at 3.5 µm, besides the lower incoming power, we are also pumping the fiber in the normal dispersion regime far from the ZDW. Consequently, soliton dynamics only occurs when SPM allows to cross the ZDW during propagation, whereas in the previous case, solitons and associated DWs are generated directly at the beginning. Thus, Raman self-frequency shift of the solitons allows to reach longer wavelengths in the mid-IR.

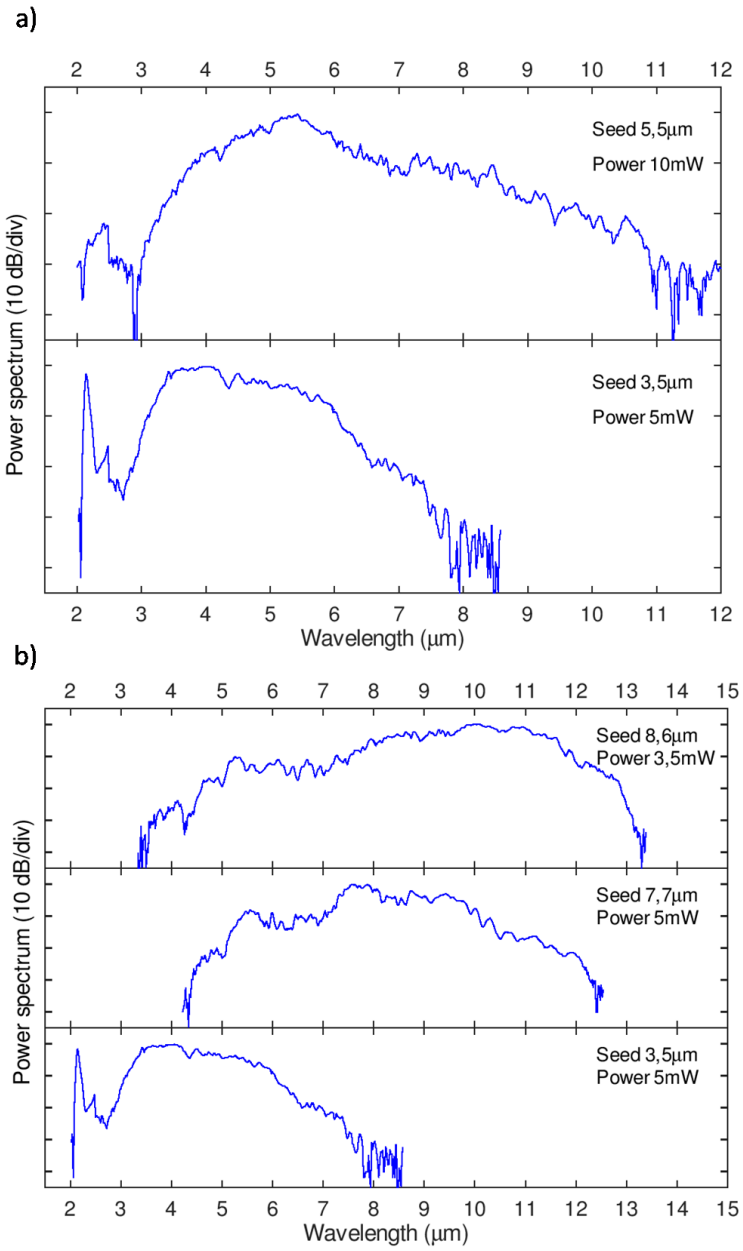

Fig.13. (a) Experimental SC spectra recorded for different pumping wavelength (3.5 and 5.5 µm) in a 12.7-µm suspended core fiber. (b) Results obtained for other pumping wavelength (3.5, 7.7 and 8.6 µm).

5. Conclusion

In conclusion, we demonstrated the experimental development of arsenic- and antimony-free chalcogenide optical fibers with low residual losses. Distinct fiber structures such as step-index or suspended-core profiles were designed and then drawn to evidence easy-accessible management of group-velocity dispersion properties. Thus, proof-of-principle SC generation experiments were carried out, and our results clearly confirm the potential of these new fibers for nonlinear optics in the mid-IR. More particularly, a SC spectrum spanning from 2 to 14 µm was obtained by using a 40-mm-long segment of 10-µm-core step-index fiber made of the

following glass pair $Ge_{20}Se_{60}Te_{20}$ / $Ge_{20}Se_{70}Te_{10}$. Despite the fact that several optimization steps are required about the fiber design and their characterization, as well as the mid-IR detection system, the present results based on this new type of chalcogenide fibers satisfying the European REACH regulation are fully comparable to the current state-of-the-art using fibers made from more common chalcogenide glasses compatible with fiber drawing.

Acknowledgments

We acknowledge the financial support of the French Investissements d'Avenir program (ISITE-BFC ANR-15-IDEX-0003 Project SCUVIRA).

6. References

[1] C. R. Petersen, N. Prtljaga, M. Farries, J. Ward, B. Napier, G. R. Lloyd, J. Nallala, N. Stone, and O. Bang, Mid-infrared multispectral tissue imaging using a chalcogenide fiber supercontinuum source, Optics letters **43**, 999–1002 (2018).

[2] Z. Zhao, B. Wu, X. Wang, Z. Pan, Z. Liu, P. Zhang, X. Shen, Q. Nie, S. Dai, and R. Wang, Mid-infrared supercontinuum covering 2.0–16 μm in a low-loss telluride single-mode fiber, Laser & Photonics Reviews **11** (2017).

[3] M. F. Ferreira, E. Castro-Camus, D. J. Ottaway, J. M. López-Higuera, X. Feng, W. Jin, Y. Jeong, N. Picqué, L. Tong, B. M. Reinhard*et al.*, Roadmap on optical sensors, Journal of Optics **19**, 083001 (2017).

[4] C. Strutynski, J. Picot-Clémente, F. Désévédavy, J.-C. Jules, G. Gadret, B. Kibler, and F. Smektala, Compact supercontinuum sources based on tellurite suspended core fibers for absorption spectroscopy beyond 2 μm, Laser Physics Letters **13**, 075402 (2016).

[5] A. Picot, L'antimoine, un vieux toxique toujours meconnu, PreventiqueSecurite pp. 30–33 (2007).

[6] B. Ljujic, L. Sundac*et al.*, [[council] directive 98/83/ec [of 3 november 1998] on the quality of water intended for human consumption: review and intregral translation [from english into serbian]], Vodaisanitarnatehnika (Serbia and Montenegro) .

[7] https://echa.europa.eu/fr/regulations/reach/legislation, .

[8] R. J. Curry, S. W. Birtwell, A. K. Mairaj, X. Feng, and D. W. Hewak, A study of environmental effects on the attenuation of chalcogenide optical fibre, Journal of Non-Crystalline Solids **351**, 477–481 (2005).

[9] F. W. Glaze, D. H. Blackburn, J. S. Osmalov, D. Hubbard, and M. H. Black, Properties of arsenic sulfide glass, Journal of Research of the National Bureau of Standards **59**, 83–92 (1957).

[10] T. Kohoutek, X. Yan, T. W. Shiosaka, S. N. Yannopoulos, A. Chrissanthopoulos, T. Suzuki, and Y. Ohishi, Enhanced raman gain of ge–ga–sb–s chalcogenide glass for highly nonlinear microstructured optical fibers, JOSA B **28**, 2284–2290 (2011).

[11] V. Shiryaev and M. Churbanov, Trends and prospects for development of chalcogenide fibers for mid-infrared transmission, Journal of Non-Crystalline Solids **377**, 225–230 (2013).

[12] T. Wang, X. Gai, W. Wei, R. Wang, Z. Yang, X. Shen, S. Madden, and B. Luther-Davies, Systematic z-scan measurements of the third order nonlinearity of chalcogenide glasses, Optical Materials Express **4**, 1011–1022 (2014).

[13] B. Zhang, Y. Yu, C. Zhai, S. Qi, Y. Wang, A. Yang, X. Gai, R. Wang, Z. Yang, and B. Luther-Davies, High brightness 2.2–12 μm mid-infrared supercontinuum generation in a nontoxic chalcogenide step-index fiber, Journal of the American Ceramic Society (2016).

[14] O. Mouawad, J. Picot-Clémente, F. Amrani, C. Strutynski, J. Fatome, B. Kibler, F. Désévédavy, G. Gadret, J.-C. Jules, D. Deng, Y. Ohishi, and F. Smektala, Multioctavemidinfraredsupercontinuum generation in suspended-core chalcogenide fibers, Opt. Lett. **39**, 2684–2687 (2014).

[15] C. R. Petersen, U. Møller, I. Kubat, B. Zhou, S. Dupont, J. Ramsay, T. Benson, S. Sujecki, N. Abdel-Moneim, Z. Tang, D. Furniss, A. Seddon, and O. Bang, Mid-infrared supercontinuum covering the 1.4–13.3 μm molecular fingerprint region using ultra-high na chalcogenide step-index fibre, Nature Photonics (2014).

[16] U. Møller, Y. Yu, I. Kubat, C. R. Petersen, X. Gai, L. Brilland, D. Méchin, C. Caillaud, J. Troles, B. Luther-Davies *et al.*, Multi-milliwatt mid-infrared supercontinuum generation in a suspended core chalcogenide fiber, Optics Express **23**, 3282–3291 (2015).

[17] H. Ou, S. Dai, P. Zhang, Z. Liu, X. Wang, F. Chen, H. Xu, B. Luo, Y. Huang, and R. Wang, Ultrabroadsupercontinuum generated from a highly nonlinear ge–sb–se fiber, Opt. Lett. **41**, 3201–3204 (2016).

[18] B. Zhang, W. Guo, Y. Yu, C. Zhai, S. Qi, A. Yang, L. Li, Z. Yang, R. Wang, D. Tang *et al.*, Low loss, high na chalcogenide glass fibers for broadband mid-infrared supercontinuum generation, Journal of the American Ceramic Society **98**, 1389–1392 (2015).

[19] Z. Zhao, X. Wang, S. Dai, Z. Pan, S. Liu, L. Sun, P. Zhang, Z. Liu, Q. Nie, X. Shen *et al.*, 1.5–14 μmmidinfraredsupercontinuum generation in a low-loss te-based chalcogenide step-index fiber, Optics letters **41**, 5222–5225 (2016).

[20] B. Wu, Z. Zhao, X. Wang, Y. Tian, N. Mi, P. Chen, Z. Xue, Z. Liu, P. Zhang, X. Shen *et al.*, Mid-infrared supercontinuum generation in a suspended-core tellurium-based chalcogenide fiber, Optical Materials Express **8**, 1341–1348 (2018).

[21] M. Chazot, M. El Amraoui, S. Morency, Y. Messaddeq, and V. Rodriguez, Investigation of the drawing region in the production of ge-si optical fibers for infrared applications, Journal of Non-Crystalline Solids (2017).

[22] C. Conseil, V. Shiryaev, S. Cui, C. Boussard-Plédel, J. Troles, A. Velmuzhov, A. Potapov, A. Suchkov, M. Churbanov, and B. Bureau, Preparation of High Purity Te-Rich Ge-Te-Se Fibers for 5-15 mu m Infrared Range, Journal of Lightwave Technology **31**, 1703–1707 (2013).

[23] S. Maurugeon, B. Bureau, C. Boussard-Pledel, A. Faber, X. Zhang, W. Geliesen, and J. Lucas, Te-rich ge–te–se glass for the co< sub> 2</sub> infrared detection at 15μm, Journal of Non-Crystalline Solids **355**, 2074–2078 (2009).

[24] S. Cui, C. Boussard-Plédel, J. Troles, and B. Bureau, Telluride glass single mode fiber for mid and far infrared filtering, Optical Materials Express **6**, 971–978 (2016).

[25] X. Jiang and A. Jha, Engineering of a ge–te–se glass fibre evanescent wave spectroscopic (fews) mid-ir chemical sensor for the analysis of food and pharmaceutical products, Sensors and Actuators B: Chemical **206**, 159–169 (2015).

[26] C. Vigreux, M. V. Thi, G. Maulion, R. Kribich, M. Barillot, V. Kirschner, and A. Pradel, Wide-range transmitting chalcogenide films and development of micro-components for infrared integrated optics applications, Optical Materials Express **4**, 1617–1631 (2014).

[27] S. Maurugeon, C. Boussard-Plédel, J. Troles, A. Faber, P. Lucas, X. Zhang, J. Lucas, and B. Bureau, Telluride glass step index fiber for the far infrared, Journal of Lightwave Technology **28**, 3358–3363 (2010).

[28] A. Wilhelm, C. Boussard-PlÃ©del, Q. Coulombier, J. Lucas, B. Bureau, and P. Lucas, Development of Far-Infrared-Transmitting Te Based Glasses Suitable for Carbon Dioxide Detection and Space Optics, Advanced Materials **19**, 3796–3800 (2007). 10.1002/adma.200700823.

[29] V. Shiryaev, J.-L. Adam, and X. Zhang, Calorimetric study of characteristic temperatures and crystallization behavior in ge–as–se–te glass system, Journal of Physics and Chemistry of Solids **65**, 1737–1744 (2004).

[30] J. Troles, V. Shiryaev, M. Churbanov, P. Houizot, L. Brilland, F. Desevedavy, F. Charpentier, T. Pain, G. Snopatin, and J. Adam, GeSe4 glass fibres with low optical losses in the mid-IR, Optical Materials **32**, 212 – 215 (2009).

[31] L. G. Aio, A. M. Efimov, and V. F. Kokorina, Refractive index of chalcogenide glasses over a wide range of compositions, Journal of Non-Crystalline Solids **27**, 299–307 (1978).

[32] P. Houizot, F. Smektala, V. Couderc, J. Troles, and L. Grossard, Selenide glass single mode optical fiber for nonlinear optics, Optical Materials **29**, 651–656 (2007). Houizot, Patrick Smektala, Frederic Couderc, Vincent Troles, Johann Grossard, Ludovic.

[33] S. Danto, P. Houizot, C. Boussard-Pledel, X. H. Zhang, F. Smektala, and J. Lucas, A Family of Far-Infrared-Transmitting Glasses in the Ga-Ge-Te System for Space Applications, Advanced Functional Materials **16**, 1847–1852 (2006). 10.1002/adfm.200500645.

[34] V. Mittal, J. S. Wilkinson, and G. S. Murugan, High-contrast gete 4 waveguides for mid-infrared biomedical sensing applications, in Integrated Optics: Devices, Materials, and Technologies XVIII, , vol. 8988 (International Society for Optics and Photonics, 2014), vol. 8988, p. 89881A.

[35] V. Q. Nguyen, J. S. Sanghera, P. Pureza, F. H. Kung, and I. D. Aggarwal, Fabrication of arsenic selenide optical fiber with low hydrogen impurities, Journal of the American Ceramic Society **85**, 2849–2851 (2002).

[36] G. Snopatin, V. Shiryaev, V. Plotnichenko, E. Dianov, and M. Churbanov, High-purity chalcogenide glasses for fiber optics, Inorganic Materials **45**, 1439–1460 (2009).

[37] V. Shiryaev and M. Churbanov, Recent advances in preparation of high-purity chalcogenide glasses for mid-ir photonics, Journal of Non-Crystalline Solids (2017).

[38] C. Strutynski, J. Picot-Clémente, A. Lemiere, P. Froidevaux, F. Désévédavy, G. Gadret, J.-C. Jules, B. Kibler, and F. Smektala, Fabrication and characterization of step-index tellurite fibers with varying numerical aperture for near- and mid-infrared nonlinear optics, J. Opt. Soc. Am. B **33**, D12–D18 (2016).

[39] J. Troles, Y. Niu, C. Duverger-Arfuso, F. Smektala, L. Brilland, V. Nazabal, V. Moizan, F. Desevedavy, and P. Houizot, Synthesis and characterization of chalcogenide glasses from the system Ga-Ge-Sb-S and preparation of a single-mode fiber at 1.55Â [mu]m, Materials Research Bulletin **43**, 976–982 (2008). Doi: DOI: 10.1016/j.materresbull.2007.04.029.

[40] P. Melman and R. Davies, Application of the clausius-mossotti equation to dispersion calculations in optical fibers, Journal of lightwave technology **3**, 1123–1124 (1985).

[41] V. S. Shiryaev, J. L. Adam, X. H. Zhang, C. Boussard-Pledel, J. Lucas, and M. F. Churbanov, Infrared fibers based on Te-As-Se glass system with low optical losses, Journal of Non-Crystalline Solids **336**, 113–119 (2004).

[42] M. El-Amraoui, G. Gadret, J. C. Jules, J. Fatome, C. Fortier, F. Désévédavy, I. Skripatchev, Y. Messaddeq, J. Troles, L. Brilland, W. Gao, T. Suzuki, Y. Ohishi, and F. Smektala, Microstructured chalcogenide optical fibers from As_2S_3 glass: towards new IR broadband sources, Opt. Express **18**, 26655–26665 (2010).

[43] M. F. Churbanov, I. Scripachev, G. E. Snopatin, V. S. Shiryaev, and V. G. Plotnichenko, High purity glasses based on arsenic chalcogenides, J. Opt. Adv. Mat **3**, 341–349 (2001).

[44] M. El-Amraoui, J. Fatome, J. C. Jules, B. Kibler, G. Gadret, C. Fortier, F. Smektala, I. Skripatchev, C. F. Polacchini, Y. Messaddeq, J. Troles, L. Brilland, M. Szpulak, and G. Renversez, Strong infrared spectral broadening in low-loss As-S chalcogenide suspended core microstructured optical fibers, OPTICS EXPRESS **18**, 4547–4556 (2010).

[45] S. Duval, J.-C. Gauthier, L.-R. Robichaud, P. Paradis, M. Olivier, V. Fortin, M. Bernier, M. Piché, and R. Vallée, Watt-level fiber-based femtosecond laser source tunable from 2.8 to 3.6 μm, Optics letters **41**, 5294–5297 (2016).

[46] http://www.femtum.com/en/products/ultrafast-laser/, .

[47] J. M. Dudley and J. R. Taylor, *Supercontinuum generation in optical fibers* (Cambridge University Press, 2010).

[48] S. Kedenburg, C. Strutynski, B. Kibler, P. Froidevaux, F. Désévédavy, G. Gadret, J.-C. Jules, T. Steinle, F. Mörz, A. Steinmann *et al.*, High repetition rate mid-infrared supercontinuum generation from 1.3 to 5.3 μm in robust step-index tellurite fibers, JOSA B **34**, 601–607 (2017).